Contribution from the Lash Miller Chemical Laboratories and Erindale College, University of Toronto, Toronto, Ontario, Canada

Rhodium and Iridium Atom Chemistry: Binary Carbonyls of Rhodium and Iridium

GEOFFREY A. OZIN* and A. J. LEE HANLAN

Received August 31, 1978

Rh and Ir atom matrix cocondensations at 10–12 K involving $^{12}C^{16}O$, $^{12}C^{16}O/^{13}C^{16}O$, $^{12}C^{16}O/^{13}C^{18}O$, and $^{12}C^{16}O$/inert gas and $^{12}C^{16}O/^{13}C^{16}O$/inert gas mixtures (Ne, Ar, Kr, Xe) are shown to give birth to the new series of binary carbonyl complexes $M(CO)_n$ (where M = Rh, Ir; n = 1, 2, 3, 4). The infrared and UV–visible spectroscopic data for $Rh(CO)_4/Ir(CO)_4$ are discussed in terms of the distortion problem originally expounded for the lighter d^9 congener, $Co(CO)_4$. Force constant trends within the $M(CO)_n$ (M = Co, Rh, Ir, Ni, Pd, Pt; n = 1–4) series are contemplated in terms of systematic alterations in metal–carbon and carbon–oxygen σ/π-orbital contributions.

Introduction

The importance of cobalt carbonyls and their derivatives as selective catalysts in a wide variety of industrial carbonylation and hydroformylation reactions has been well documented,[1,2] and although not widely used in industry, rhodium carbonyl complexes have exhibited even higher reactivities and selectivities, under milder conditions, when used as catalysts for the oxo reaction.[3] Coordinatively unsaturated metal carbonyl species have been proposed as the active catalytic intermediates in these various processes[2] and have also been postulated as active sites in a variety of polymer-supported transition-metal catalyst systems.[4] In this vein, the behavior of CO molecules chemisorbed on supported Rh[5–7,38–46] and Ir[38–46] catalysts has been the subject of several infrared studies. From these studies it has been proposed that distinct sites for chemisorbed CO exist on these metals, for example, RhCO, $Rh(CO)_2$, Rh_2CO, Ir(CO), and $Ir(CO)_2$.[5–8,38–46]

One possible method for gaining some insight into the molecular and electronic properties and the reactivities of these species may be the examination of the analogous coordinatively unsaturated binary carbonyls, $M(CO)_n$. For the cobalt triad of the group 8 transition metals, the only information to appear in the literature has dealt exclusively with the binary carbonyls of cobalt; no corresponding data are available for rhodium or iridium.

Unlike $Ni(CO)_4$,[9] cobalt tetracarbonyl cannot be easily prepared or stored at room temperature. In 1965 Keller and Wawersik[10] first obtained $Co(CO)_4$ as a paramagnetic species by sublimation of $Co_2(CO)_8$ onto a 77 K cold finger held in the microwave cavity of an ESR spectrometer. By Knudsen cell pyrolysis of $Co_2(CO)_8$, Bidinosti and McIntyre[11] were able to detect $Co(CO)_4$ mass spectrometrically. In addition to these syntheses, two independent groups have formed $Co(CO)_4$ in CO or CO/Ar matrices at 10–20 K. Rest et al.[12] photolyzed $Co(CO)_3NO$ in the presence of CO at 20 K while Ozin et al.[13] cocondensed cobalt vapor and CO onto an optical window held at 10–12 K; both methods led to the spectroscopic identification of $Co(CO)_4$. Matrix infrared isotopic substitution experiments[12,13] along with Raman[13] and ESR[10,13,14] data have indicated that $Co(CO)_4$ undergoes distortion away from a regular tetrahedral geometry. Together with vibrational isotope calculations,[12,13] the data appear to favor a geometry consistent with a C_{3v} symmetry. This experimental finding was in contrast to EHMO and angular overlap molecular orbital analyses by Hoffmann[15] and Burdett,[16] who determined that a D_{2d} structure should be slightly favored for the d^9 $Co(CO)_4$ molecule. In addition to $Co(CO)_4$, the synthesis and vibrational data for the lower binary carbonyls $Co(CO)_m$ (where m = 1–3) have also been reported.[13]

Aside from a brief report by this research group,[17] there has been no account of the corresponding preparation of the rhodium and iridium binary carbonyls. When we considered the homogeneous and heterogeneous catalytic implications of the carbonyl complexes of these metals, it seemed appropriate to attempt the metal atom matrix synthesis of $M(CO)_n$ species, where M = Rh or Ir and n = 1–4. In this paper the synthesis and characterization of these complexes are evaluated with particular attention to their comparison with the corresponding cobalt species.

Results and Discussion

Tetracarbonyls of Cobalt, Rhodium, and Iridium. The d^{10} tetracarbonyls of the group 8 metals Ni,[18,22] Pd,[19–21] and Pt[19–24] have been found to take on regular tetrahedral (T_d) symmetry when formed under matrix isolation conditions in both pure CO and CO/Ar matrices. One would not, however, necessarily expect the d^9 Co, Rh, and Ir analogues to behave similarly, since Jahn–Teller instability may cause distortions away from the most regular structures.[23]

It has been shown with vibrational, ESR, and electronic spectroscopies that $Co(CO)_4$[13] undergoes a C_{3v} trigonal distortion. In what follows, it will be ascertained that the nature of the spectroscopic data for the analogous $Rh(CO)_4$ and $Ir(CO)_4$ species makes it difficult to distinguish unequivocally between a regular tetrahedral or a slightly distorted tetrahedral geometry.

Tetracarbonyl Rhodium, $Rh(CO)_4$. When rhodium atoms were cocondensed with pure $^{12}C^{16}O$ under the same conditions which, with cobalt, resulted in formation of $Co(CO)_4$ (i.e., $M/CO \simeq 1/10^4$), a doublet was observed in the CO stretching region of the infrared spectrum at 2019 and 2012 cm^{-1} (Figure 1). The relative intensities of these two bands remained essentially invariant during a number of different runs and during matrix warm-up experiments; they were therefore assigned to a single absorbing species. If one assumes that, analogous to cobalt, the $Rh(CO)_4$ molecule was formed under these conditions in pure CO matrices, then it is interesting to note that the doublet splitting of 7 cm^{-1} was considerably less than the 18-cm^{-1} split observed for $Co(CO)_4$, which was attributed to a genuine distortion of the complex superimposed on a matrix site effect.[13]

In order to determine if this 7-cm^{-1} split in $Rh(CO)_4$ reflects a molecular distortion of a tetrahedral molecule, as in the case of $Co(CO)_4$,[13] or simply a matrix site effect originating in the low C_2 substitutional site symmetry of crystalline CO, or a multiple trapping site effect (as in the case of $Pt(CO)_4$),[22] it was necessary to study the formation of $Rh(CO)_4$ in a variety of dilute CO matrices. Some interesting behavior was observed for the doublet band when several pure CO and CO/Ar experiments were compared (Figure 2). In $CO/Ar \simeq 1/10$ and pure CO matrices the main component of the doublet often appeared split itself, while in other cases of similar resolution the main doublet seemed poorly resolved or virtually absent. This behavior indicates that the original splitting may be due to a multiple trapping site effect rather than a molecular distortion and that the ν(CO) region of the $Rh(CO)_4$ molecule is extremely sensitive to the matrix environment. Evidence in favor of a genuine distortion, however, arises from a comparison of the magnitude of the band splitting for samples

0020-1669/79/1318-2091$01.00/0

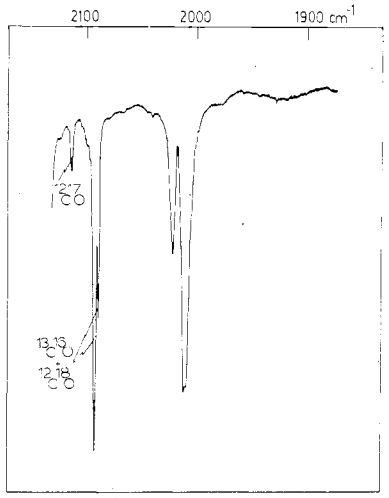

Figure 1. Matrix infrared spectrum of the products of the cocondensation reaction of Rh atoms with pure CO (where Rh/CO ≃ 1/10⁴) at 10–12 K.

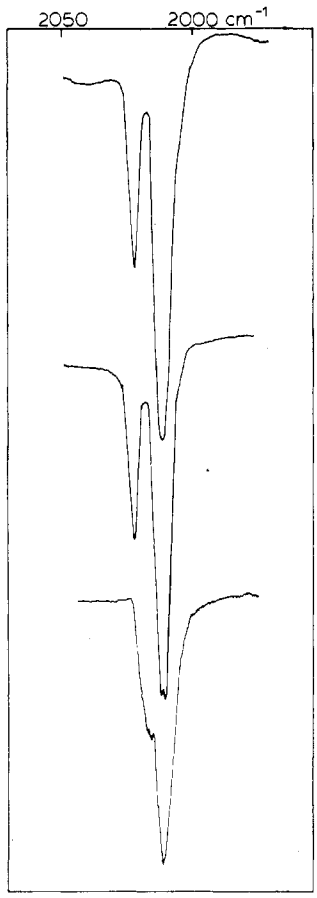

Figure 2. Illustration of the various splitting patterns observed for the 2019/2012 cm^{-1} doublet in (A) pure CO, (B) CO/Ar ≃ 1/10, showing an additional split of the main 2012-cm^{-1} component, and (C) pure CO, showing the high-frequency component only as a shoulder.

of $Rh(CO)_4$ formed in CO, Ne, Ar, Kr, and Xe matrices. Figure 3 graphs the frequencies of the two components of the doublet as a function of the matrix polarizabilities,[24] where it can be observed that the magnitude of the splitting remains roughly constant (7–10 cm^{-1}) in all five matrices. Extrapolation of these data to zero polarizability yields a "gas phase splitting" value of about 10 cm^{-1}, suggesting that a genuine molecular distortion exists for $Rh(CO)_4$. Comparison with similar data for the cobalt complex (Figure 4) indicates that

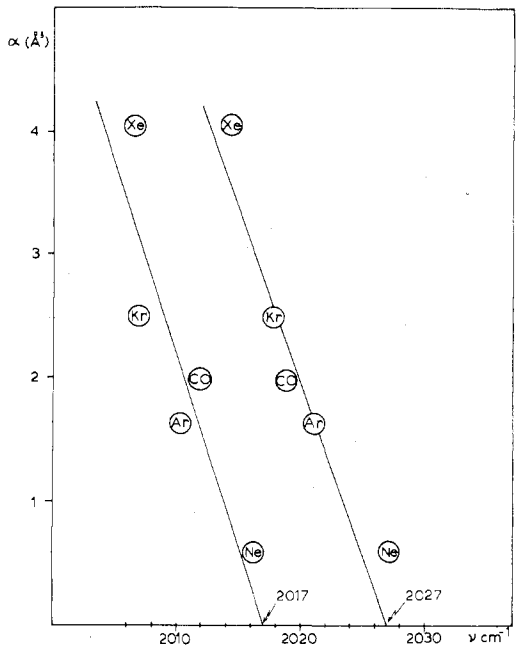

Figure 3. Plot of polarizability (α, Å^3) vs. frequency (ν, cm^{-1}) for the two CO stretching modes of $Rh(CO)_4$ in Ne, Ar, Kr, Xe, and CO matrices.

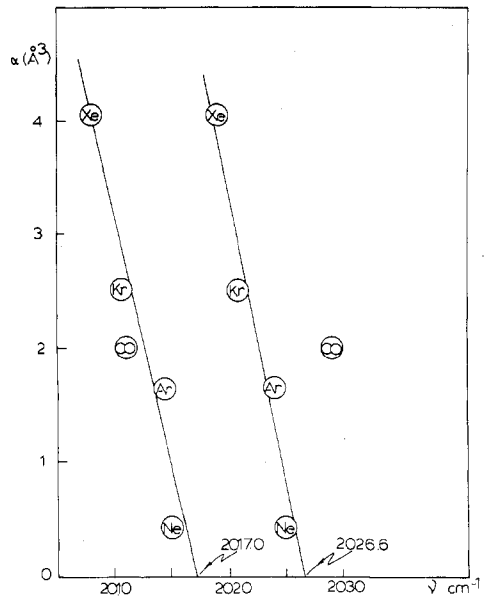

Figure 4. Same as Figure 3 but for $Co(CO)_4$.

the magnitude of the splitting was approximately the same for $Rh(CO)_4$ and $Co(CO)_4$ in all matrices except pure CO, where the larger split for $Co(CO)_4$ was attributed to the combination of a molecular distortion and a site perturbation. Such a rationale, however, does not seem to be appropriate for $Rh(CO)_4$ where the insensitivity of the splitting to various matrices implies a common molecular distortion of the molecule.

To further delve into the type of distortion experienced by $Rh(CO)_4$ and to verify the molecular stoichiometry, we cocondensed rhodium atoms with $^{12}C^{16}O/^{13}C^{16}O$ (45/55) mixtures. From Figure 5 it can be seen that the original doublet at 2019/2012 cm^{-1}, representing the $^{12}C^{16}O$ complex, produced a similar doublet, shifted to 1973/1967 cm^{-1}, corresponding to the $^{13}C^{16}O$ isotopically substituted species. In addition, *at least four other bands* were observed to fall in the region between the two doublets and were assigned to the various mixed $^{12}C^{16}O/^{13}C^{16}O$ molecules. Since only five

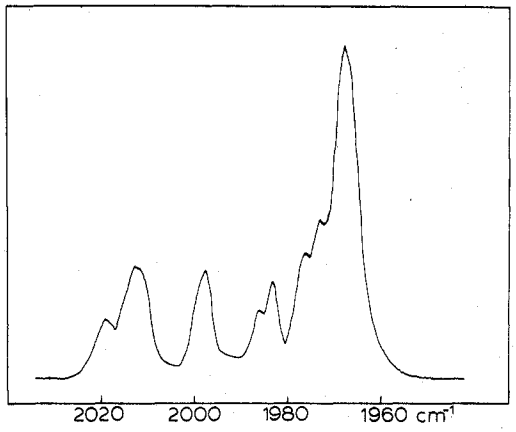

Figure 5. Matrix infrared spectrum of $Rh(^{12}C^{16}O)_n(^{13}C^{16}O)_{4-n}$ (where n = 0–4), resulting from the cocondensation reaction of Rh atoms with $^{12}C^{16}O/^{13}C^{16}O \simeq 45/55$ mixtures at 10–12 K.

isotopic frequencies are expected in this region for a regular tetrahedral $M(^{12}C^{16}O)_n(^{13}C^{16}O)_{4-n}$ system (where n = 0–4; see for example $Pd(CO)_4$ and $Pt(CO)_4$[19-22]), the mixed isotopic data support the hypothesis that $Rh(CO)_4$ may be somewhat distorted from a regular tetrahedral geometry. In view of the C_{3v} distortion which was deduced for $Co(CO)_4$,[13] a similar model was assumed for $Rh(CO)_4$ and frequency calculations were performed[25] by using a Cotton–Kraihanzel force field approximation.[26] The $^{12}C^{16}O/^{13}C^{16}O$ isotopic substitution leads to eight molecules which must be considered, and adjustment of the four force constant parameters k_{CO}, $k_{CO'}$, $k_{CO\cdot CO'}$, and $k_{CO'\cdot CO'}$, gave the best fit frequencies for a C_{3v} geometry. The results of the calculation are given in Table I.

In light of the matrix sensitivity observed for the original doublet, as displayed in some pure CO and CO/Ar experiments discussed earlier, and to cover all possibilities, a calculation was also performed for a regular tetrahedral molecule. On the assumption that the 2019/2012, 1986/1983, and 1973/1967 cm^{-1} doublets were due to matrix perturbations, it was necessary to obtain the best frequency fit by using a set of frequencies involving only one component for each doublet. The best fit of the calculated and observed frequencies and the calculated force constants, k_{CO} and $k_{CO\cdot CO'}$, was obtained with the observed set of frequencies as listed in Table II.

On comparison of the calculated and observed frequencies and standard deviations for the C_{3v} and T_d models (Tables I and II), a somewhat better fit was observed for the tetrahedral geometry. We believe, however, that the difference in the two models was not significant enough to allow a distinct conclusion to be made on the molecular geometry at this point.

In an attempt to confirm the preferred geometry, additional isotope data were obtained by reactions with a mixture of $^{12}C^{16}O$ (43%)/$^{13}C^{18}O$ (47.9%)/$^{12}C^{18}O$ (4.6%)/$^{13}C^{16}O$ (2.7%). The observed spectrum is shown in Figure 6. Calculated spectra were obtained for both the T_d and C_{3v} models by using the resultant force constants obtained from the previous calculations performed on the $^{12}C^{16}O/^{13}C^{16}O$ isotope data (Tables I and II). No attempt was made at a least-squares fit of these observed and calculated spectra due to the abundance of absorptions. The results of the calculations are displayed in stick form for T_d and C_{3v} symmetry, where the intensity was approximated to be proportional to the statistical abundance of each possible molecule, on the basis of the isotope percentage of the gas mixture. Once again it can be seen that both the T_d and C_{3v} symmetry models produce calculated spectra that fit reasonably well to those observed.

The results of the isotopic substitution experiments and frequency calculations, as well as the behavior of the bands in dilute CO matrices, are inconclusive with respect to molecular geometry. Although we are confident with a ligand stoichiometry of four, it is not possible, based on the vibrational spectroscopic data, to unambiguously distinguish between a regular tetrahedral geometry and one which is distorted toward C_{3v} symmetry. That some of the evidence does favor a distortion suggests that the $Rh(CO)_4$ molecule may experience a slight departure from tetrahedral symmetry but most likely to a smaller extent than was observed for $Co(CO)_4$.[13]

Table I. Observed and Calculated Infrared Frequencies for $Rh(^{12}C^{16}O)_n(^{13}C^{16}O)_{4-n}$ (Where n = 0–4), C_{3v} Model

	IR, cm^{-1}		symmetry assignt
	obsd	calcd	
molecule I		2096.27[a]	A_1
$Rh(^{12}C^{16}O)_4$	2019.0	2018.60	A_1
C_{3v}	2012.0	2011.83	E
molecule II		2087.11[a]	A_1
$Rh(^{13}C^{16}O)(^{12}C^{16}O)_3$	2012.0	2011.83	E
C_{3v}	1983.2	1982.88	A_1
molecule III		2088.73[a]	A_1'
$Rh(^{13}C^{16}O)(^{12}C^{16}O)_3$	2019.0	2017.86	A_1'
C_s	2012.0	2011.83	A_1''
	1976.0	1975.42	A_1''
molecule IV		2080.18[a]	A_1'
$Rh(^{12}C^{16}O)_2(^{13}C^{16}O)_2$	2019.0	2016.42	A_1'
C_s	1986.0	1984.95	A_1'
	1967.0	1967.58	A_1''
molecule V		2078.01[a]	A_1'
$Rh(^{13}C^{16}O)_2(^{12}C^{16}O)_2$	2012.0	2011.83	A_1''
C_s	1986.0	1987.93	A_1'
	1972.5	1971.17	A_1''
molecule VI		2066.79[a]	A_1'
$Rh(^{12}C^{16}O)(^{13}C^{16}O)_3$	1997.5	1996.70	A_1'
C_s	1972.5	1973.17	A_1'
	1967.0	1967.58	A_1'
molecule VII		2070.10[a]	A_1
$Rh(^{12}C^{16}O)(^{13}C^{16}O)_3$	1997.5	1999.16	A_1
C_{3v}	1967.0	1967.58	E
molecule VIII		2050.17[a]	A_1
$Rh(^{13}C^{16}O)_4$	1972.5	1974.21	A_1
C_{3v}	1967.0	1967.58	E

Force Constants (mdyn/Å): k_{CO} = 16.84, $k_{CO'}$ = 16.70, $k_{CO\cdot CO'}$ = 0.34, $k_{CO'\cdot CO'}$ = 0.34

Standard Deviation: 0.55581×10^{-5}

[a] Overlap with intense $^{12}C^{16}O$ or $^{13}C^{16}O$ bands and/or too weak to observe.

Table II. Observed and Calculated Infrared Frequencies for $Rh(^{12}C^{16}O)_n(^{13}C^{16}O)_{4-n}$ (Where n = 0–4), T_d Model

	IR, cm^{-1}		symmetry assignt
	obsd	calcd	
molecule I	2012.0	2011.62	T_2
$Rh(^{12}C^{16}O)_4$			
T_d			
molecule II		2149.67[a]	A_1
$Rh(^{12}C^{16}O)_3(^{13}C^{16}O)$	2012.0	2011.62	E
C_{3v}	1976.0	1976.14	A_1
molecule III		2139.01[a]	A_1
$Rh(^{12}C^{16}O)_2(^{13}C^{16}O)_2$	2012.0	2011.62	B_1
C_{2v}	1986.0	1985.99	A_1
	1967.0	1967.39	B_2
molecule IV		2126.75[a]	A_1
$Rh(^{12}C^{16}O)(^{13}C^{16}O)_3$	1997.6	1997.44	A_1
C_{3v}	1967.0	1967.39	E
molecule V	1967.0	1967.39	T_2
$Rh(^{13}C^{16}O)_4$			
T_d			

Force Constants (mdyn/Å): k_{CO} = 16.97, $k_{CO\cdot CO}$ = 0.62

Standard Deviation: 0.56068×10^{-6}

[a] Overlap with intense $^{12}C^{16}O$ line and/or too weak to be observed.

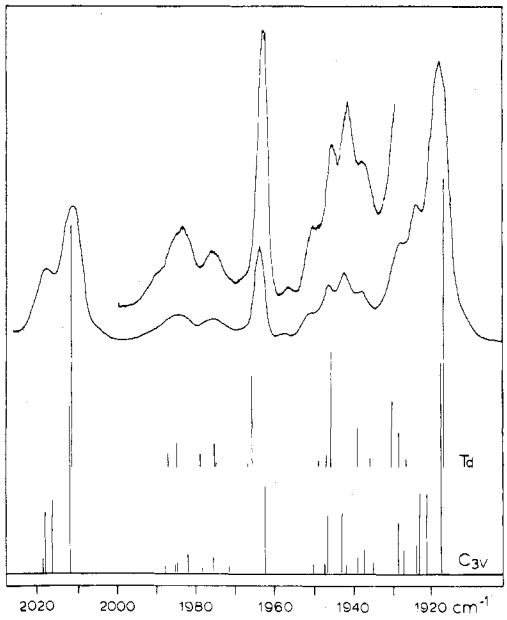

Figure 6. Matrix infrared spectrum of the products of the cocondensation reaction of Rh atoms with mixtures of $^{12}C^{16}O/^{13}C^{18}O/^{12}C^{18}O/^{13}C^{16}O \simeq 43/47.9/4.6/2.7$, compared with stick representations of calculated spectra by using T_d and C_{3v} symmetry models. Calculated intensities were approximated to be proportional to the statistical abundance of each molecule, on the basis of the isotope percentages of the gas mixture.

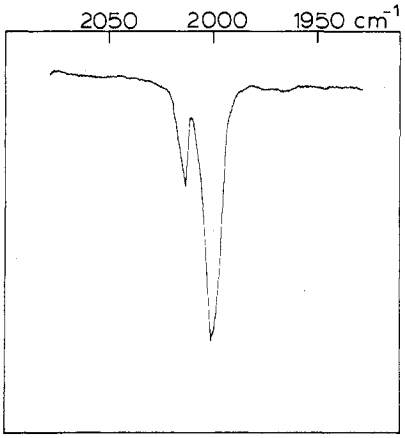

Figure 7. Matrix infrared spectrum of the products of the reaction of Ir atoms and pure CO (where $Ir/CO \simeq 1/10^4$) at 10–12 K.

Tetracarbonyl Iridium, $Ir(CO)_4$. To complete the investigation of the tetracarbonyls of the cobalt triad, iridium atoms were cocondensed with pure CO matrices at a dilution of $Ir/CO \simeq 1/10^4$. The resulting spectrum shown in Figure 7, aside from an 11-cm^{-1} *red shift*, was virtually identical with that obtained with Rh and CO, displaying a doublet at 2008.4/2001.3 cm^{-1}. The band splitting of approximately 7 cm^{-1} was the same as that observed for $Rh(CO)_4$ and so it was strongly suspected that an analogous $Ir(CO)_4$ species was formed which would prove to be isostructural to the rhodium complex. The $^{12}C^{16}O/^{13}C^{16}O$ isotopic substitution experiments confirmed this suspicion, as the spectrum shown in Figure 8 closely parallels that of the $Rh(^{12}C^{16}O)_n(^{13}C^{16}O)_{4-n}$ carbonyls. The iridium $^{13}C^{16}O$ isotopically substituted complex gave a corresponding, but less clearly resolved, doublet at 1961/1956.2 cm^{-1}, with essentially four other bands present for the mixed isotope species.

Considering the similarities of the $Rh(CO)_4$ and $Ir(CO)_4$ infrared spectra, we performed analogous frequency calculations for the iridium molecule as for the rhodium species,

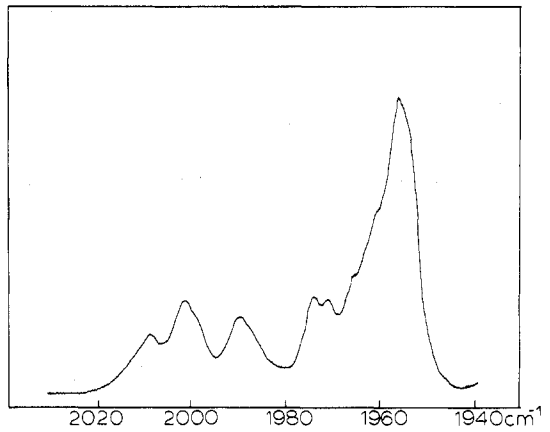

Figure 8. Matrix infrared spectrum of $Ir(^{12}C^{16}O)_n(^{13}C^{16}O)_{4-n}$ (where $n = 0$–4) resulting from the cocondensation reaction of Ir atoms with $^{12}C^{16}O/^{13}C^{16}O \simeq 45/55$ mixtures at 10–12 K.

Table III. Observed and Calculated Infrared Frequencies for $Ir(^{12}C^{16}O)_n(^{13}C^{16}O)_{4-n}$ (Where $n = 0$–4), C_{3v} Model

	IR, cm^{-1}		symmetry assignt
	obsd	calcd	
molecule I		2100.54[a]	A_1
$Ir(^{12}C^{16}O)_4$	2008.4	2007.28	A_1
C_{3v}	2001.3	2000.91	E
molecule II		2091.75[a]	A_1
$Ir(^{13}C^{16}O)(^{12}C^{16}O)_3$	2001.3	2000.91	E
C_{3v}	1970.8	1971.39	A_1
molecule III		2082.25[a]	A_1'
$Ir(^{13}C^{16}O)(^{12}C^{16}O)_3$	2008.4	2006.63	A_1'
C_s	2001.3	2000.91	A_1''
	1965.5	1965.30	A_1'
molecule IV		2082.86[a]	A_1'
$Ir(^{12}C^{16}O)_2(^{13}C^{16}O)_2$	2008.4	2005.36	A_1'
C_s	1974.2	1975.41	A_1'
	1956.2	1956.91	A_1''
molecule V		2082.08[a]	A_1'
$Ir(^{13}C^{16}O)_2(^{12}C^{16}O)_2$	2001.3	2000.91	A_1''
C_s	1974.2	1976.96	A_1'
	1961.0	1960.45	A_1'
molecule VI		2070.42[a]	A_1'
$Ir(^{12}C^{16}O)(^{13}C^{16}O)_3$	1989.6	1986.28	A_1'
C_s	1961.0	1962.25	A_1'
	1956.2	1956.91	A_1''
molecule VII		2071.74[a]	A_1
$Ir(^{12}C^{16}O)(^{13}C^{16}O)_3$	1989.6	1990.43	A_1
C_{3v}	1956.2	1956.91	E
molecule VIII		2054.35[a]	A_1
$Ir(^{13}C^{16}O)_4$	1961.0	1963.13	A_1
C_{3v}	1956.2	1956.91	E

Force Constants (mdyn/Å): $k_{CO} = 16.69$, $k_{CO'} = 16.60$, $k_{CO\cdot CO'} = 0.39$, $k_{CO'\cdot CO'} = 0.41$

Standard Deviation: 0.10286×10^{-4}

[a] Overlap with intense $^{12}C^{16}O$ or $^{13}C^{16}O$ lines and/or too weak to observe.

using C_{3v} and T_d symmetry models. The best fit of calculated and observed frequencies and resultant force constants is shown in Tables III and IV. It is interesting to note that for the T_d $Ir(CO)_4$ calculation the best fit of observed and calculated frequencies was obtained with the corresponding set of components of the split bands, as was found for $Rh(CO)_4$.

The results of the observed and calculated spectra for the $^{12}C^{16}O/^{13}C^{18}O/^{12}C^{18}O/^{13}C^{16}O$ isotopic substitution experiment are compared in Figure 9 where only subtle differences occur between the C_{3v} and T_d models, such that either one presents a reasonable representation of the observed spectrum.

Once again, the ambiguity of the vibrational data does not allow a definite conclusion on the molecular geometry of $Ir(CO)_4$ to be reached.

Table IV. Observed and Calculated Infrared Frequencies for $Ir(^{12}C^{16}O)_n(^{13}C^{16}O)_{4-n}$ (Where n = 0-4), T_d Model

	IR, cm^{-1} obsd	IR, cm^{-1} calcd	symmetry assignt
molecule I	2001.3	2000.75	T_2
$Ir(^{12}C^{16}O)_4$			
T_d			
molecule II		2187.29[a]	A_1
$Ir(^{12}C^{16}O)_3(^{13}C^{16}O)$	2001.3	2000.75	E
C_{3v}	1965.5	1965.94	A_1
molecule III		2163.09[a]	A_1
$Ir(^{12}C^{16}O)_2(^{13}C^{16}O)_2$	2001.3	2000.75	B_1
C_{2v}	1974.2	1976.05	A_1
	1956.2	1956.76	B_2
molecule IV		2163.61[a]	A_1
$Ir(^{12}C^{16}O)(^{13}C^{16}O)_3$	1989.6	1987.45	A_1
C_{3v}	1956.2	1956.76	E
molecule V	1956.2	1956.76	T_2
$Ir(^{13}C^{16}O)_4$			
T_d			

Force Constants (mdyn/Å): $k_{CO} = 17.01, k_{CO\cdot CO} = 0.835$

Standard Deviation: 0.61131×10^{-5}

[a] Overlap with intense $^{12}C^{16}O$ line and/or too weak to be observed.

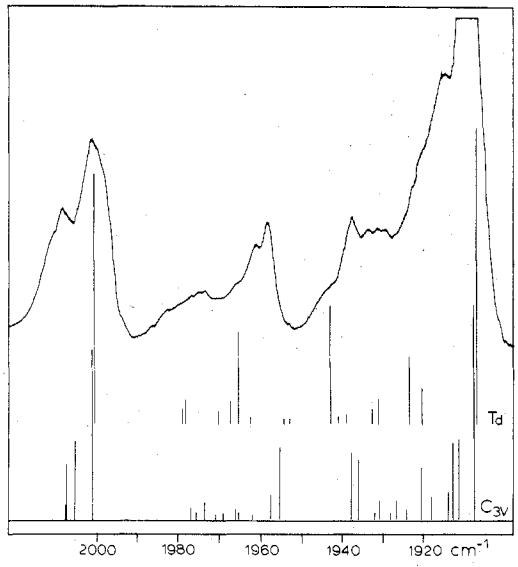

Figure 9. Matrix infrared spectrum of the products of the cocondensation reaction of Ir atoms with $^{12}C^{16}O/^{13}C^{18}O/^{12}C^{18}O/^{13}C^{16}O$, compared with stick representations of calculated spectra by using T_d and C_{3v} symmetry models. Isotope percentages and calculation of intensities were as in Figure 6.

Metal–Ligand Stretching Modes. The observation and assignment of lines in the metal–ligand stretching region of the infrared spectrum for matrix-isolated binary carbonyls was problematic because of their low extinction coefficients compared to the relatively high values of the corresponding CO stretching modes. Very weak absorptions in this low-frequency region, however, were observed for all three tetracarbonyls of the cobalt triad when their respective CO stretching modes were nearly fully absorbing.

It has been previously reported[13] that $Co(CO)_4$ exhibits weak bands at 552 and 486 cm^{-1}, which by analogy to $Ni(CO)_4$[22] were assigned to the δ(Co–CO) mode and the ν(Co–C) stretch, respectively, the latter being the most intense of the two bands (cf. 459 and 423 cm^{-1}, respectively, for $Ni(CO)_4$[22]). For $Rh(CO)_4$, two weak bands were observed at 439 and 420 cm^{-1} and may be tentatively assigned to δ(Rh–CO) and ν(Rh–C), respectively; once again the lower-frequency band was the more intense. Only one band was assigned in the case of $Ir(CO)_4$ at 410 cm^{-1} and may be attributed to the ν(Ir–C) stretching mode.

Table V. Metal–Ligand Force Constant and Frequency Data for $M(CO)_4$ (Where M = Co, Rh, Ir, Ni, Pd, and Pt)

	freq obsd, cm^{-1}	assignt	k_{M-C},[a] mdyn/Å
Co	552	δ(M–CO)	
	486	ν(M–C)	2.42
Rh	438	δ(M–CO)	
	420	ν(M–C)	2.13
Ir	410	ν(M–C)	2.32
Ni[b]	435	ν(M–C)	1.80
Pd[b]	258	ν(M–C)	0.82
Pt	304	ν(M–C)	1.28

[a] Determined by using the approximation that treats $M(CO)_4$ as a T_d MX_4 molecule with mass of X = 28. [b] From ref 19-22.

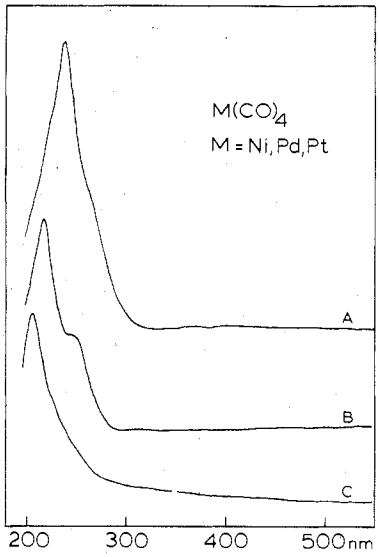

Figure 10. Matrix optical spectra of (A) $Ni(CO)_4$, (B) $Pd(CO)_4$, and (C) $Pt(CO)_4$, observed when the respective metal atoms were cocondensed with pure CO at 10–12 K, showing the MLCT regions of the $M(CO)_4$ complexes.

It was not possible to obtain calculated M–C bond stretching force constants from the limited frequency data. However, k_{M-C} values could be estimated by considering each of the $M(CO)_4$ molecules to be approximated by a tetrahedral $M(X_4)$ molecule (where X has the same mass as CO) and by using the equation:

$$\lambda_{T_2} = k_{M-C}[\mu_x + {}^4/_3\mu_M]$$

where μ_x and μ_M are the reciprocal masses of $^{12}C^{16}O$ and the metal atom, respectively. The k_{M-C} values obtained for each of cobalt, rhodium, and iridium tetracarbonyl are summarized in Table V. These and other force constant trends are discussed in a later section.

Optical Spectra of Metal Tetracarbonyls. Before we discuss the electronic spectra of the cobalt, rhodium, and iridium d^9 open shell tetracarbonyls, it is appropriate for purposes of comparison to first discuss the d^{10} tetracarbonyls of the nickel triad, which have been shown to have a regular tetrahedral geometry.[19-22]

Nickel, Palladium, and Platinum Tetracarbonyls. The observed electronic spectra for the nickel, palladium, and platinum tetracarbonyls, as shown in Figure 10, exhibit a single intense absorption band in the ultraviolet region with, in the case of nickel and palladium, a well-pronounced shoulder 5000–6000 cm^{-1} to lower energy (Table VI).[27]

The photoelectron spectrum of $Ni(CO)_4$ has been reported[28] and several molecular orbital treatments have appeared.[29] From these there is a general agreement that the highest filled orbitals are the e and t_2 of the d manifold, separated by about

Table VI. Electronic Spectral Data for $M(CO)_4$ Molecules (Where M = Ni, Pd, Pt, Co, Rh, and Ir)

metal	freq obsd nm	freq obsd cm^{-1}	assignt
Ni	273	36 630	$t_2(d) \rightarrow t_2(\pi^*)$
	240	41 666	$d \rightarrow \pi^*$
Pd	250	40 000 sh	$t_2(d) \rightarrow t_2(\pi^*)$
	218	45 872	$d \rightarrow \pi^*$
Pt	207	48 310	$d \rightarrow p$ or $d \rightarrow \pi^*$
Co	355	28 169	$\sigma \rightarrow t_2(d)$
	346	28 902 sh	$\sigma \rightarrow t_2(d)$
	315	31 746	$\sigma \rightarrow t_2(d)$
	269	37 175 sh	$d \rightarrow \pi^*$
	256	39 063	$d \rightarrow \pi^*$
	223	44 843	$d \rightarrow \pi^*$
Rh[a]	335	29 851	$\sigma \rightarrow t_2(d)$
	240	41 667 sh	$d \rightarrow \pi^*$
	215	46 511	$d \rightarrow \pi^*$
Ir	307	32 573	$\sigma \rightarrow t_2(d)$
	246	40 650 sh	$d \rightarrow \pi^*$
	208	48 077	$d \rightarrow \pi^*$

[a] $Rh(CO)_4$ bands displayed slight matrix concentration and temperature-dependent energy shifts, possibly due to an overlap of $Rh(CO)_4/Rh_2(CO)_8$; see text.

5000 cm^{-1}, with the latter at higher energy. The next level is composed primarily of the σ-bonding orbitals of the carbonyl groups and lies about 35 000 cm^{-1} below the filled e level; transitions from this level are not expected below 50 000 cm^{-1}. The splitting of the lowest unoccupied orbitals, t_2, e, and t_1, which arises from the interaction among π^* states of each CO ligand, is expected to be small. In hexacarbonyls,[30] the splitting is of the order of 5000–7000 cm^{-1}, with a smaller splitting expected for tetracarbonyls since the CO groups are further apart in a tetrahedral array than in an octahedral one, therefore decreasing their mutual interaction. One can subsequently envisage a plethora of allowed metal-to-ligand charge-transfer (MLCT) transitions from the e and t_2 levels into the e, t_1, and t_2 components of the carbonyl π^* levels, at very similar energy.

It is therefore proposed[27] that the low-energy shoulder in $Ni(CO)_4$ and $Pd(CO)_4$ be assigned to $t_2(d) \rightarrow t_2(\pi^*)$, as the latter orbitals should be stabilized by mixing with metal p functions. The intense band at higher energy most probably represents several overlapping transitions with $t_2(d) \rightarrow t_2(\pi^*)$ and $e(d) \rightarrow \pi^*$ character. A more detailed assignment is not possible.

The apparent absence of the low-energy shoulder in the $Pt(CO)_4$ spectrum may imply that the $t_2(d) \rightarrow t_2(\pi^*)$ transition has shifted to higher energy. Indeed, the band at 48 310 cm^{-1} may represent $t_2(d) \rightarrow t_2(\pi^*)$. Alternatively, the 48 310-cm^{-1} band could be primarily a $d \rightarrow p$ type transition, i.e., $e(d) \rightarrow t_2(\pi^*)$. Such $d \rightarrow p$ transitions have often been observed in the ultraviolet spectrum of platinum complexes.[31]

Cobalt, Rhodium, and Iridium Tetracarbonyls. While the complexes described previously are closed-shell, 18-electron, regular tetrahedral species, the cobalt series possesses 17 electrons and is not necessarily regularly shaped. Infrared and ESR data[13,14] have indicated that $Co(CO)_4$ has a marked C_{3v} distortion, while the rhodium and iridium carbonyls appear to be more closely tetrahedral, or at least distorted to a lesser degree. The electronic spectra of these complexes, to be described, support assigning a lesser distortion to the Rh and Ir complexes compared to that of the cobalt species. From Figure 11 it can be seen that $Co(CO)_4$ has a spectrum in which the features observed for the rhodium and iridium analogue appear to have been doubled. The high-energy ultraviolet band of $Co(CO)_4$ is split by about 2000 cm^{-1} while the pair of near-ultraviolet bands are separated by nearly 3000 cm^{-1}, with the lower-energy band revealing a shoulder. Close examination

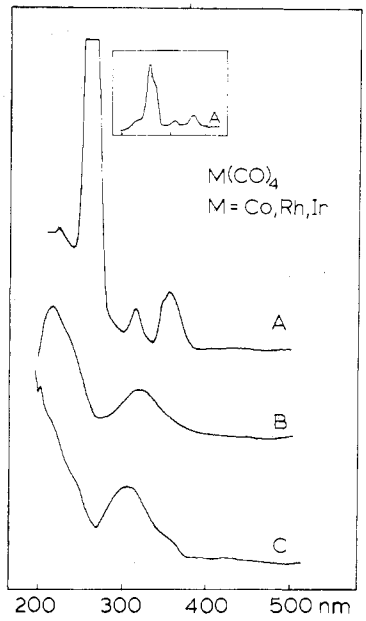

Figure 11. Matrix optical spectra of (A) $Co(CO)_4$, (B) $Rh(CO)_4$, and (C) $Ir(CO)_4$ observed when the respective metal atoms were cocondensed with pure CO at 10–12 K, showing the MLCT and LMCT regions of the $M(CO)_4$ complexes.

of the spectrum of $Rh(CO)_4$ reveals a low-energy shoulder on the high-energy band. The low-energy band is very broad and could conceivably encompass several transitions. $Ir(CO)_4$ exhibits a band which appears to peak just below the 200-nm cutoff of the UV–visible spectrometer, with shoulders evident on the low-energy side. The broad, low-energy band of $Ir(CO)_4$ also appears to have a slight shoulder and may represent multiple transitions. The observed optical transitions for the cobalt, rhodium, and iridium tetracarbonyls are summarized in Table VI.

Turning first to the peaks some 10 000–17 000 cm^{-1} below the main band, we can see that there are two for $Co(CO)_4$ separated by about 3000 cm^{-1} but only one for each of $Rh(CO)_4$ and $Ir(CO)_4$. It had previously been claimed[13] that the two observed low-energy bands in $Co(CO)_4$ were best assigned to d–d transitions. Such an assignment would set the split of the d manifold at about 30 000 cm^{-1}, highly unlikely in view of molecular orbital treatments and photoelectron spectral data for $Ni(CO)_4$ which imply a split of approximately 5000 cm^{-1} for that molecule.[28a] A sixfold increase in the crystal field splitting on passing from Ni to Co cannot be justified.[27] The absence of similar low-energy bands in the electronic spectra of the nickel, palladium, and platinum tetracarbonyls suggested that their presence in the cobalt group may be due to the hole in the t_2 metal set of d orbitals.[27] For this reason it is proposed that these low-energy bands be assigned to ligand-to-metal charge-transfer (LMCT) transitions originating from the bonding σ carbonyl level into the hole of the d orbital manifold in the metal, i.e., $\sigma t_2(CO) \rightarrow t_2(d)$. The vertical energy separation between these levels was seen in $Ni(CO)_4$ from the photoelectron spectrum[28] to be about 42 000 cm^{-1}; since the metal t_2 subshell is closed, no transition is observed. The transition, possible in the cobalt series, is expected to occur well below 42 000 cm^{-1}. Such a transition would decrease the electron repulsion energy in the carbonyl σ orbitals and give rise to a considerable exchange energy stabilization through the formation of a closed d shell in the excited state. Observation of such LMCT bands in the region of 30 000 cm^{-1} seems appropriate.

The existence of two such bands for $Co(CO)_4$ compared to one broad band for each of $Rh(CO)_4$ and $Ir(CO)_4$ is perhaps most easily explained by assigning different geometries to the

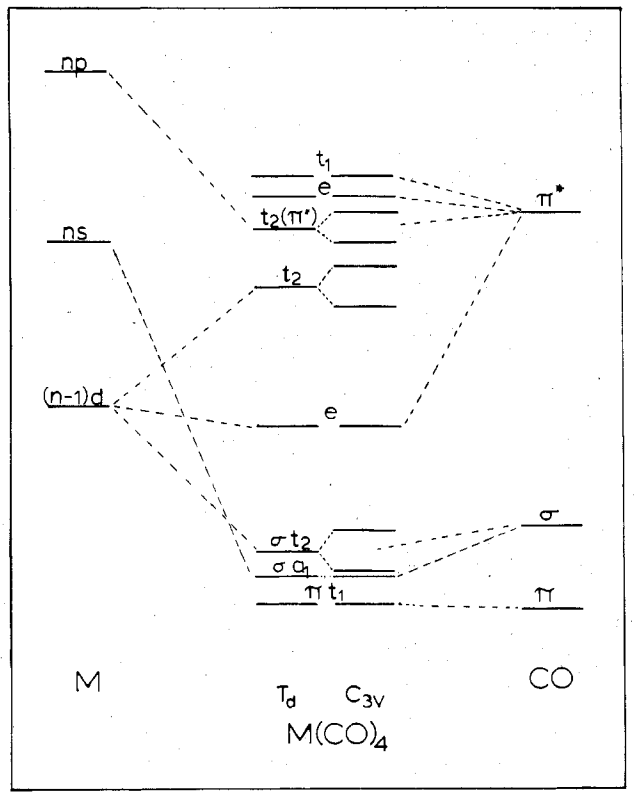

Figure 12. Qualitative MO energy level scheme for T_d and C_{3v} $M(CO)_4$ binary carbonyl complexes. (Note that under C_{3v} symmetry t_1 also splits to e + a_1.)

two groups. Figure 12 qualitatively illustrates the effects that a C_{3v} perturbation will have on the energy levels of a T_d $M(CO)_4$ system. The t_2 levels are expected to split into e and a_1 levels with the σ orbitals likely to be perturbed in the lower (C_{3v}) symmetry to a greater degree than the π^* set. For this reason the two near-ultraviolet bands of $Co(CO)_4$ ($^2A_1$ ground state in C_{3v} symmetry) are assigned to the LMCT transitions $a_1 \rightarrow a_1$ ($^2A_1 \rightarrow {}^2A_1$) and $e \rightarrow a_1$($^2A_1 \rightarrow {}^2E$). The higher intensity and slight splitting observed in the lower energy band is consistent with its assignment to the latter transition.

For the rhodium and iridium tetracarbonyls, where only a single broad band is observed in the near-ultraviolet region, both geometries may be considered. For T_d symmetry one LMCT transition is allowed, from the t_2(M–C) σ level to the hole in the t_2 metal set, consistent with the observed data. However, if the complexes are distorted toward a C_{3v} symmetry, but to a lesser degree than $Co(CO)_4$, then the splitting of the t_2 orbitals, to a_1 and e levels, will be expected to be less, in which case the two allowed LMCT transitions $a_1 \rightarrow a_1$ and $e \rightarrow a_1$ will lie very close in energy, possibly coalescing to give one broad band. This is also consistent with observation.

Because of the closed-shell nature of most $M(CO)_x$ complexes and the relatively low energies of the CO binding levels, LMCT transitions have been rarely mentioned in analyses of metal carbonyl optical data. Molecules with open-shell ground states are likely places to look for LMCT bands, as demonstrated here and in an earlier report that suggested that a broad high-energy absorption in the spectrum of $V(CO)_6$ represents a transition from the $t_{1g}(\sigma)$ level to the hole in the t_{2g}(d) level.[31]

The intense high-energy bands of the cobalt, rhodium, and iridium tetracarbonyls can be assigned to $d \rightarrow \pi^*$ MLCT transitions, following the arguments used for the species of the nickel group. The lower C_{3v} symmetry, however, results in a splitting of the various t_2 and t_1 levels into e and a_1 components (Figure 12). In the π^* levels this splitting may only add to the number of close-lying levels, thereby increasing the

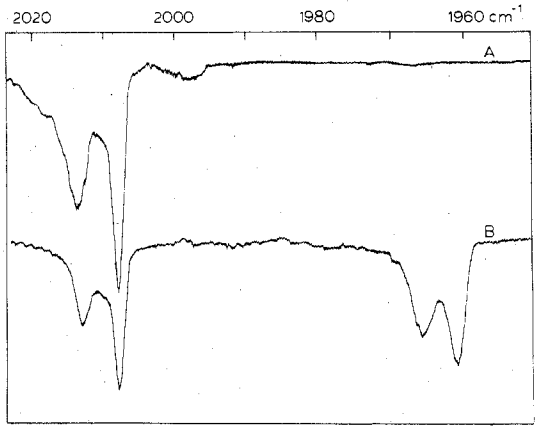

Figure 13. Matrix infrared spectrum of the products of the cocondensation reaction of Rh atoms with (A) CO/Ar mixtures (1/500 dilutions) and (B) $^{12}C^{16}O/^{13}C^{16}O/Ar \simeq 1/1/500$ mixtures at 10–12 K, showing the $Rh^{12}C^{16}O$ and $Rh^{13}C^{16}O$ molecules.

plethora of possible overlapping transitions. The well-pronounced shoulders on the low- and high-energy sides of the intense band for $Co(CO)_4$, as opposed to less well-resolved shoulders in the case of $Rh(CO)_4$ and $Ir(CO)_4$, are perhaps best regarded as a manifestation of a greater degree of distortion experienced by the $Co(CO)_4$ molecule. A more precise assignment of these MLCT transitions is not possible with the limited information available.

The optical data for $Co(CO)_4$ appear to be compatible with the proposed C_{3v} distortion, while once again it is difficult to make a distinction between a tetrahedral geometry and a *slight* distortion to C_{3v} symmetry for the $Rh(CO)_4$ and $Ir(CO)_4$ molecules.

From an overall comparison of the vibrational and electronic data for the cobalt, rhodium, and iridium tetracarbonyls, it seems safe to conclude that the complexes of the latter two metals have a geometry that differs slightly from that of $Co(CO)_4$.

Intermediate Binary Carbonyls of Rhodium and Iridium. $Rh(CO)_m$ (Where m = 1–3). Isolation and identification of the intermediate binary rhodium carbonyls were severely complicated by the very narrow frequency range (12 cm^{-1}) within which the CO stretching modes for all the $Rh(CO)_{1-4}$ molecules were observed. A similar problem had been previously encountered with the platinum carbonyls,[22] whereas the analogous $Co(CO)_{1-4}$ molecules[13] were spread out over an approximate 100-cm^{-1} frequency range.

For the isolation of the lowest stoichiometry rhodium–carbonyl complex, rhodium atoms were cocondensed with $^{12}C^{16}O$ under high dilution in argon. Using these conditions we observed a well-resolved doublet at 2012.8 and 2008.0 cm^{-1} as shown in Figure 13A. Similar experimental conditions, with an isotopic mixture of $^{12}C^{16}O/^{13}C^{16}O/Ar$ (~1/1/500) produced a corresponding doublet in the $^{13}C^{16}O$ region of the spectrum at 1965.6 and 1960.8 cm^{-1} (Figure 13B), therefore establishing that each component of the original 2012.8/2008.0 cm^{-1} doublet has a single $^{13}C^{16}O$ counterpart. This doublet of doublets is a characteristic pattern of a monocarbonyl species[13,32] where the bands at 2012.8/2008.0 and 1965.6/1960.8 cm^{-1} were assigned to the $Rh^{12}C^{16}O$ and $Rh^{13}C^{16}O$ molecules, respectively. The two components of the doublets, separated by ~4.8 cm^{-1}, are most likely due to a multiple trapping site effect reflecting slightly different matrix environments for the RhCO molecule. To calculate the primary stretching CO force constant for rhodium monocarbonyl, we did two separate calculations, one for each component of the doublet and its isotope counterpart. Using a Cotton–Kraihanzel force field approximation[26] and obtaining the best fit of observed and calculated frequencies,[25] we calculated CO

Table VII. Observed and Calculated Infrared Frequencies for Both Sites of Rh(CO)

molecule	IR, cm^{-1} obsd	calcd
(1) $Rh(^{12}C^{16}O)$	2012.8	2011.31
$Rh(^{13}C^{16}O)$	1965.6	1967.09
(2) $Rh(^{12}C^{16}O)$	2008.0	2006.51
$Rh(^{13}C^{16}O)$	1960.8	1962.39

Force Constants (mdyn/Å): $k_{CO}(1) = 16.35$, $k_{CO}(2) = 16.27$, $k_{CO}^{av} = 16.30$

Standard Deviation: 0.12592×10^{-4}

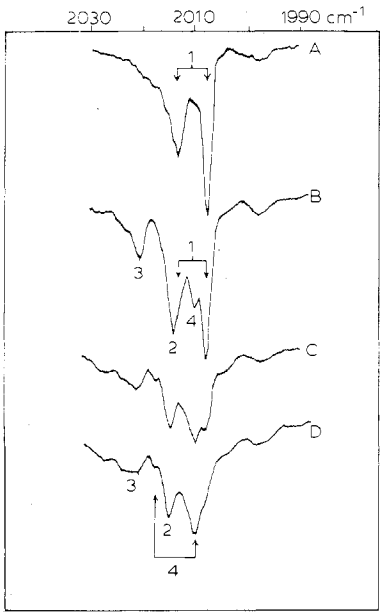

Figure 14. The infrared spectrum (A) as in Figure 13A at 6 K, (B), (C), and (D) after warming to 20, 35, and 40 K, respectively (where 4 = $Rh(CO)_4$, 3 = $Rh(CO)_3$, 2 = $Rh(CO)_2$ and 1 = Rh(CO)).

force constants at 16.35 mdyn/Å for the 2012.8-cm^{-1} site and 16.27 mdyn/Å for the 2008.0-cm^{-1} site, giving an average k_{CO} value of 16.31 mdyn/Å (Table VII).

When the dilute $^{12}C^{16}O$/Ar matrix (Figure 14A) was slowly warmed in the range 10–40 K, the spectral changes shown in Figure 14B–D were observed. On warming of the matrix to 20 K the intensity of the high-frequency 2012.8-cm^{-1} component of the RhCO doublet significantly increased and in fact shifted to a slightly higher frequency of 2014 cm^{-1}, while the 2008.0-cm^{-1} band did not increase to the same extent. This would suggest that a new species has grown in at ~2014 cm^{-1}, overlapping with the high-energy component of the monocarbonyl. In addition to these changes, *two new bands* appeared at 2010 and 2020 cm^{-1}. Warming to 35 K (Figure 14C) resulted in a sharp decrease of the intensity of the low-energy 2008-cm^{-1} component of RhCO while the 2012.8-cm^{-1} component was very small and hidden by the new 2014-cm^{-1} band. The 2010-cm^{-1} band continued to grow and occurred at a frequency expected for the tetracarbonyl (2012/2019 cm^{-1} in pure CO) but slightly shifted in dilute matrices. The high-energy component of the tetracarbonyl was barely visible at about 2018 cm^{-1}. By 40 K (Figure 14D) the monocarbonyl had essentially disappeared, leaving the tetracarbonyl at 2010/2018 cm^{-1} and two bands at 2014.8 and 2020 cm^{-1}. One could anticipate that these two bands belonged to the remaining intermediate binary carbonyls $Rh(CO)_2$ and $Rh(CO)_3$. Which band should be assigned to which molecule was not clear despite several warm-up experiments. Additional *information* was obtained from a similar warm-up analysis of the $^{12}C^{16}O/^{13}C^{16}O$/Ar isotopic spectrum shown in Figure 15.

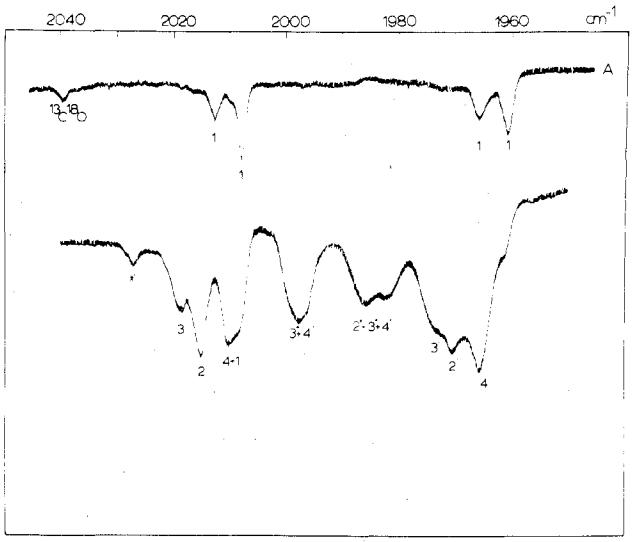

Figure 15. Matrix infrared spectrum of the products of the co-condensation reaction of Rh atoms with $^{12}C^{16}O/^{13}C^{16}O$/Ar (A) as in Figure 13B at 10–12 K and (B) after warming to 40 K. The asterisk indicates an impurity line.

Table VIII. Observed and Calculated Infrared Frequencies for $Rh(^{12}C^{16}O)_q(^{13}C^{16}O)_{2-q}$ (Where q = 0–2)

molecule	IR, cm^{-1} obsd	calcd[a]
$Rh(^{12}C^{16}O)_2$	2014.6	2014.46
$Rh(^{12}C^{16}O)(^{13}C^{16}O)$	1984.0	1983.99
$Rh(^{13}C^{16}O)_2$	1970.0	1970.16

Force Constants (mdyn/Å): $k_{CO} = 16.84$, $k_{CO\cdot CO} = 0.44$

Standard Deviation 0.81618×10^{-7}

[a] Based on a $D_{\infty h}$ geometry for $Rh(CO)_2$.

Table IX. Observed and Calculated Infrared Frequencies for $Rh(^{12}C^{16}O)_p(^{13}C^{16}O)_{3-p}$ (Where p = 0–3)

molecule	IR, cm^{-1} obsd	calcd[a]
$Rh(^{12}C^{16}O)_3$	2018.4	2018.10
$Rh(^{12}C^{16}O)_2(^{13}C^{16}O)$	2018.4	2018.10
	1984.0	1984.10
$Rh(^{12}C^{16}O)(^{13}C^{16}O)_2$	1997.5	1997.41
	1973.4	1973.72
$Rh(^{13}C^{16}O)_3$	1973.4	1973.72

Force Constants (mdyn/Å): $k_{CO} = 16.95$, $k_{CO\cdot CO} = 0.49$

Standard Deviation: 0.39749×10^{-6}

[a] Based on a D_{3h} geometry.

At 40 K all four binary carbonyls were present but the isotopic spectrum was complicated by multiple band overlaps due to the narrow frequency range for the CO stretching modes of the various molecules. The assignments for all the isotopic molecules, as shown in Figure 15B, were supported by frequency and force field calculations. The best fit of the observed and calculated frequencies and the resultant force constants for $Rh(CO)_2$ and $Rh(CO)_3$ are given in Tables VIII and IX, respectively.

$Ir(CO)_m$ (Where m = 1–3). The parallel behavior displayed so far in the reactions of Rh and Ir with CO prompted the investigation of the lower stoichiometry iridium carbonyls. However, on cocondensing of iridium with dilute CO/Ar (1/100–1/500) matrices, a very different spectrum was obtained (Figure 16A) compared to that observed for similar Rh experiments (Figure 13), the iridium spectrum displaying four bands in the CO stretching region compared to the RhCO

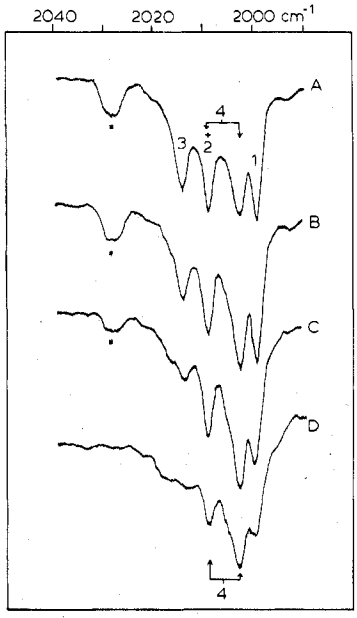

Figure 16. Matrix infrared spectrum of the cocondensation reaction of Ir atoms with CO/Ar mixtures (1/500 dilutions) (A) at 10–12 K and (B), (C), and (D) after warming to 20, 30, and 35 K, respectively (where 4 = $Ir(CO)_4$, 3 = $Ir(CO)_3$, 2 = $Ir(CO)_2$, and 1 = Ir(CO)). The asterisk indicates an impurity.

doublet. It would appear, therefore, that under these dilution conditions IrCO was not isolated exclusively but occurred in the presence of all the lower binary carbonyls.

Deciphering the IR data for the lower stoichiometry complexes was again complicated by the narrow frequency range (10 cm^{-1}) within which the ν(CO) bands occurred. Information leading to band assignments was obtained, however, from careful warm-up experiments during which the growth and decay behavior of the ν(CO) absorptions was monitored.

When the matrix in Figure 16A was carefully warmed to 20 K (Figure 16B), the bands at 1999.5 and 2009 cm^{-1} remained relatively unchanged, while the band at 2002.6 cm^{-1} increased slightly and that at 2014.2 cm^{-1} decreased. At 30 K a considerable decrease in the 1999.5- and 2014.2-cm^{-1} bands was observed while the 2002.6-cm^{-1} absorption increased and the 2009-cm^{-1} band again remained unchanged (Figure 16C). At 35 K the spectrum was dominated by the 2009/2002.6 cm^{-1} doublet with a portion of each of the 1999.5- and 2014.2-cm^{-1} bands remaining (Figure 16D). The predominance of the 2009/2002.6 cm^{-1} doublet at the highest temperature suggests that it is the highest stoichiometry $Ir(CO)_4$ complex. In pure CO matrices the tetracarbonyl was observed as a doublet at 2008.4/2001.3 cm^{-1} consistent with the assignment of the similar 2009/2002.6 cm^{-1} doublet of $Ir(CO)_4$ but slightly shifted in dilute matrices.

Since IrCO was not formed exclusively in the matrix, it was not possible to obtain unambiguous confirmation of stoichiometry. For this reason assignment of IrCO and the remaining intermediate carbonyls was made on the basis of the warm-up behavior and by analogy to the rhodium carbonyl system. This leads to assignment of IrCO, $Ir(CO)_2$, and $Ir(CO)_3$ as indicated in Figure 16 and summarized in Table X.

The inability to trap IrCO exclusively within the confines of the matrix, under conditions which allowed for isolation of RhCO and CoCO, was believed to be primarily due to a temperature effect. The higher melting point of iridium compared to that of rhodium would necessarily result in a higher radiation flux from the vapor source transmitted to the matrix during deposition and after solidification. The slightly warmer temperature felt by the matrix during deposition would then allow formation of the higher stoichiometry iridium carbonyls in addition to the monocarbonyl species.

Table X. Infrared Frequencies for the Binary Carbonyls of Iridium, $Ir(CO)_p$ (Where p = 1–3)

obsd freq, cm^{-1}	molecular assignt
2014.2	$Ir(CO)_3$
2009.0	$Ir(CO)_2$
1999.5	Ir(CO)

Geometries of the Lower Binary Carbonyls. For both the MCO and $M(CO)_2$ binary carbonyls of Co, Rh, and Ir, linear geometries were assumed for purposes of calculating force constant data. A linear, $D_{\infty h}$ geometry for $M(CO)_2$ species has been predicted by EHMO and angular overlap molecular orbital analyses as done by Hoffmann[15] and Burdett.[16]

For the tricarbonyl complex, Hoffmann's[15] analysis predicted that a C_{3v} trigonal-pyramidal geometry would be favored by both d^{10} and d^9 $M(CO)_3$ species. The pyramid was expected to be nearly flat (θ = 98 and 105° for d^{10} and d^9 species, respectively) with a computed energy of roughly 1 kcal/mol lower than that of a D_{3h} trigonal-planar structure. Burdett's[16] calculations, on the other hand, found d^{10} $M(CO)_3$ species to favor a D_{3h} planar geometry, while d^9 complexes experienced an anticipated Jahn–Teller distortion to a C_{2v} planar structure. Up to this time, infrared data for all known d^{10} tricarbonyl and related systems, $Ni(CO)_3$,[32] $Pd(N_2)_3$,[32,33] $Pt(N_2)_3$,[34] $Pd(CO)_3$,[35] and $Pt(CO)_3$,[22] agree with Burdett's prediction of planar D_{3h} geometries.

The planarity (or nonplanarity) of $M(CO)_3$ species (D_{3h} or C_{3v}) is usually determined by the nonobservation (or observation) of the totally symmetric CO stretching vibration in the infrared spectrum. However, for a near-planar structure, the symmetric CO stretching vibration is expected to be very weak compared to its asymmetric counterpart and may pass undetected in the infrared spectrum. For a planar C_{2v} molecule, as predicted by Burdett[16] for d^9 Jahn–Teller distorted $M(CO)_3$ species, the IR-active E′ mode of D_{3h} splits into A_1 and B_2. The B_2 mode may be expected to be the strongest while the A_1 component, depending on the extent of angle change in the molecule, could lie close in energy to B_2. It is possible, therefore, that only a slight splitting or band broadening may occur, making it difficult to confirm the presence of the A_1 band and hence an indicator of C_{2v} symmetry (see, for example, the $Ag(CO)_3$ molecule[36]).

The reported vibrational data for $Co(CO)_3$ favored assignment of a D_{3h} geometry for that molecule;[13] however, the ESR data[13] favored a C_{3v} pyramidal structure, as calculated by Hoffmann.[15] For the corresponding $Rh(CO)_3$ and $Ir(CO)_3$ molecules, only one infrared band was detected for each and ESR data were not obtained. Although the vibrational data for $Rh(CO)_3$ produced a reasonable frequency fit and acceptable force constants on the basis of a D_{3h} geometry (Table IX), the limited information does not allow one to arrive at a definite conclusion for the geometry of the $M(CO)_3$ rhodium and iridium complexes.

Force Constant Trends and Bonding Properties. After characterization of the binary carbonyls of Rh and Ir, $M(CO)_n$ (where n = 1–4), it is of interest to examine the trends in the available force constant data and to compare them to those previously obtained for the cobalt carbonyl complexes.[13] As has been discussed in the preceding sections of this paper, the vibrational and electronic data suggest that the geometry of $Co(CO)_4$ differs somewhat from that of the corresponding Rh and Ir complexes, all of which may be removed by some degree from a regular tetrahedral geometry. By first examining the expected force constant trends for the Ni, Pd and Pt binary carbonyls, where the three tetracarbonyls have been shown

Table XI. Cotton–Kraihanzel CO Bond Stretching Force Constants for $M(CO)_n$ (Where M = Ni, Pd, Pt and n = 1–4)

	n	k_{CO}, mdyn/Å	$k_{CO\cdot CO}$, mdyn/Å
$Ni(CO)_n$[a]	1	16.09	
	2	16.63	1.0
	3	17.00	0.57
	4	17.42	0.32
$Pd(CO)_n$[b]	1	16.97	
	2	17.16	0.29
	3	17.35	0.21
	4	17.55	0.24
$Pt(CO)_n$[c]	1	17.02	
	2	17.18	0.08
	3	17.24	0.28
	4	17.28	0.26

[a] References 32 and 35. [b] References 19 and 22. [c] Reference 22.

Table XII. Best Fit Cotton–Kraihanzel CO Stretching Force Constants[a] for the Binary Carbonyls $M(CO)_n$ (Where for M = Co and Rh, n = 1–4, and for M = Ir, n = 4)

molecule	k_{CO}	$k_{CO\cdot CO}$	$k_{CO'}$	$k_{CO'\cdot CO'}$[b]
$Co(CO)_4$ C_{3v}	16.95	0.43	16.76	0.33
$Co(CO)_3$	16.61	0.71		
$Co(CO)_2$	16.05	1.15		
Co(CO)	15.40			
$Rh(CO)_4$ T_d	16.97	0.62		
C_{3v}	16.84	0.34	16.70	0.34
$Rh(CO)_3$	16.95	0.49		
$Rh(CO)_2$	16.84	0.44		
Rh(CO)	16.31			
$Ir(CO)_4$ T_d	17.01	0.83		
C_{3v}	16.69	0.39	16.60	0.41

[a] In mdyn/Å. [b] Apply only to the C_{3v} calculations for $M(CO)_4$ in pure CO matrices.

to be isostructural,[22] and then comparing them with those of the cobalt metal triad, we gain additional information to support or refute an argument which thus far favors a different degree of distortion for the rhodium and iridium tetracarbonyls from that of $Co(CO)_4$.

In each of the Ni, Pd, and Pt series of binary carbonyls, $M(CO)_n$ (where n = 1–4), a monotonic increase in k_{CO} was observed on passing from the monocarbonyl, MCO, to the tetracarbonyl, $M(CO)_4$ (Table XI). From simple MO bonding theory one expects that as the coordination number increases the metal–carbon π-bond strength should decrease, while the CO π-bond strength increases, since the $d_\pi \rightarrow \pi^*$ interaction is bonding with respect to the M–C bond but antibonding in the CO region. At the same time, charge donation from the 5σ orbital of CO (mainly localized on the carbon, but slightly antibonding with respect to the CO bond) to the metal is likely to decrease (charge accumulation or electroneutrality ideas) resulting in a concomitant weakening of the CO bond strength. Thus the CO σ effects oppose the π effects. The monotonic increase of k_{CO} values (from MCO to $M(CO)_4$) as observed for the nickel, palladium, and platinum carbonyls would therefore indicate that the π effects dominate. This CO force constant order is not necessarily reflected by the stretching frequencies, since for $M(CO)_{2-4}$ these depend on both stretch and stretch–stretch interaction force constants, while that of MCO depends only on the stretch force constant. The observed monotonic increase in k_{CO} values for the $Ni(CO)_n$, $Pd(CO)_n$, and $Pt(CO)_n$ (n = 1–4) complexes can therefore be rationalized. Table XII and Figure 17 illustrate the observed trends in k_{CO} values for $Co(CO)_n$ (where n = 1–4 and for n = 4, C_{3v} geometry) and $Rh(CO)_n$ (where n = 1–4 and for n = 4, C_{3v} and T_d geometries). The anticipated increase in k_{CO} was observed for the binary cobalt carbonyls, while the expected order was only observed for the Rh species if one considered the value of a T_d $Rh(CO)_4$ molecule. Under C_{3v} symmetry the calculated k_{CO} value for $Rh(CO)_4$ is less than that of $Rh(CO)_3$, suggesting, in view of the Ni, Pd, Pt, and Co trends, that the fit of the vibrational data for $Rh(CO)_4$ to a C_{3v} symmetry may not generate a realistic CO bond stretching force constant.

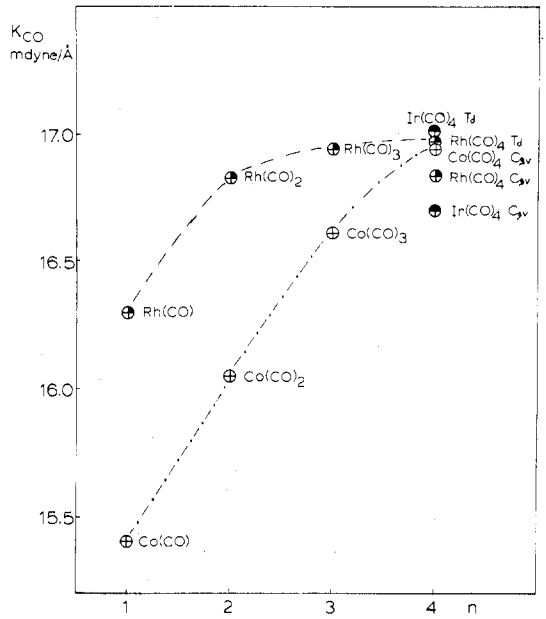

Figure 17. Graphical representation of the Cotton–Kraihanzel CO bond stretching force constants for $M(CO)_n$ (where for M = Co, Rh, n = 1–4, and for M = Ir, n = 4).

Table XIII. Comparison of the Infrared Frequencies of the Tetracarbonyl Radicals $M(CO)_4$ (Where M = Ni, Pd, Pt, Co, Rh, Ir) and the Tetracarbonylate Anions $M(CO)_4^-$ (Where M = Co, Rh, Ir)

$M(CO)_4$		$M(CO)_4^-$[a]		$M(CO)_4$[a,b]	
M	IR, cm^{-1}	M	IR, cm^{-1}	M	IR, cm^{-1}
Co	2029/2011	Co	1890	Ni	2052
Rh	2019/2012	Rh	1900	Pd	2070
Ir	2008/2001	Ir	1898	Pt	2053

[a] References 33 and 37. [b] References 19–22.

For the purposes of completion we have compiled in Table XIII the ν(CO) stretching frequencies of $M(CO)_4^-$, for M = Co, Rh, and Ir. As expected, the tetracarbonylate anions absorb at lower energies than their neutral parents, which themselves absorb at lower energies than the corresponding members of the nickel triad (effective nuclear charge arguments).

Experimental Section

Rhodium atoms were generated by directly heating a rhodium filament (0.010 in.) or by heating a tungsten rod around which either Rh sheet (0.005 in.), Rh foil (0.001 in.), or Rh wire (0.20 in.) had been wound. Iridium atoms were generated from a tungsten rod around which Ir wire (0.20 in.) had been wound. All Rh and Ir metal was supplied by A. D. McKay of New York. Research grade $^{12}C^{16}O$ (99.999%) and Ne, Ar, Kr, Xe (99.999%) were supplied by Matheson. Isotopically enriched $^{13}C^{16}O$ and $^{13}C^{18}O$ were obtained from Stohler Isotopes, Montreal. Rhodium was evaporated as previously described[21] and metal deposition rates were monitored by using a quartz crystal microbalance.[47] CsI plates for the infrared and NaCl plates for the UV–visible experiments were cooled to 6 K by an Air Products liquid-helium transfer system or to 10–12 K by an Air Products Displex closed-cycle helium refrigerator. Spectra were recorded on a Perkin-Elmer 180 for the infrared and either a Unicam SP 8000 or a Varian Techtron 635 for the UV–visible experiments.

Acknowledgment. The financial assistance of the National Research Council of Canada's New Ideas, Strategic Energy

and Operating Grants Programmes, Imperial Oil of Canada, the Atkinson Foundation, the Connaught Foundation, Erindale College, and the Lash Miller Chemical Laboratories is gratefully appreciated. A.J.L.H. acknowledges the NRCC for a scholarship throughout the duration of her graduate research. We wish also to acknowledge extremely helpful discussions with Professors A. B. P. Lever and H. B. Gray on the subject of the optical spectra of metal tetracarbonyls.

Registry No. $Rh(CO)_4$, 28132-77-6; $Ir(CO)_4$, 28132-78-7; $Co(CO)_4$, 58207-38-8; $Pt(CO)_4$, 36344-81-7; $Ni(CO)_4$, 13463-39-3; $Pd(CO)_4$, 36344-80-6; Rh(CO), 66586-41-2; $Rh(CO)_2$, 66454-17-9; $Rh(CO)_3$, 15655-05-7; $Ir(CO)_3$, 70281-27-5; $Ir(CO)_2$, 70281-28-6; Ir(CO), 70281-29-7; $Co(CO)_3$, 58168-83-5; $Co(CO)_2$, 58168-85-7; Co(CO), 58168-84-6.

References and Notes

(1) D. T. Thompson and R. Whyman in "Transition Metals in Homogeneous Catalysis", G. N. Schrauzer, Ed., Marcel Dekker, New York, 1971.
(2) (a) A. J. Chalk and J. F. Harrod, *Adv. Organomet. Chem.*, **6**, 119 (1968); (b) R. Whyman, *J. Organomet. Chem.*, **81**, 97 (1974).
(3) P. Pino, F. Piacenti, and M. Bianchi, "Organic Synthesis Via Metal Carbonyls", Vol. 2, I. Wender and P. Pino, Eds., Wiley-Interscience, New York, 1977.
(4) (a) E. O. Evans, C. U. Pittman, Jr., R. McMillan, R. T. Beach, and R. Jones, *J. Organomet. Chem.*, **67**, 295 (1974); (b) "Organometallic Polymers", C. E. Carraher, Jr., J. E. Sheats, and C. U. Pittman, Jr., Eds., Academic Press, New York, 1978.
(5) A. C. Yang and C. W. Garland, *J. Chem. Phys.*, **61**, 1504 (1975).
(6) H. Arai and H. Tominaga, *J. Catal.*, **43**, 131 (1976).
(7) H. C. Yao and W. G. Rothschild, *J. Chem. Phys.*, **68**, 4774 (1978).
(8) R. F. Howe, *J. Catal.*, **50**, 196 (1977).
(9) L. Mond, H. Hirtz, and M. D. Cowap, *J. Chem. Soc.*, **97**, 798 (1910).
(10) H. J. Keller and H. Wawersik, *Z. Naturforsch.*, **206**, 938 (1965).
(11) D. R. Bidinosti and N. S. McIntyre, *Chem. Commun.*, 1 (1967).
(12) O. Crichton, M. Poliakoff, A. J. Rest, and J. J. Turner, *J. Chem. Soc., Dalton Trans.*, 1321 (1973).
(13) L. Hanlan, H. Huber, E. P. Kündig, B. R. McGarvey, and G. A. Ozin, *J. Am. Chem. Soc.*, **97**, 7054 (1975).
(14) S. A. Fieldhouse, B. W. Fullam, G. W. Neilson, and M. C. R. Symons, *J. Chem. Soc., Dalton Trans.*, 567 (1974).
(15) M. Elian and R. Hoffmann, *Inorg. Chem.*, **14**, 1058 (1975).
(16) J. K. Burdett, *J. Chem. Soc., Faraday Trans. 2*, **70**, 1599 (1974).
(17) A. J. L. Hanlan and G. A. Ozin, *Ber. Bunsenges. Phys. Chem.*, **82**, 101 (1978).
(18) R. L. DeKock, *Inorg. Chem.*, **10**, 1205 (1971).
(19) E. P. Kündig, M. Moskovits, and G. A. Ozin, *Can. J. Chem.*, **50**, 3587 (1972).
(20) J. H. Darling and J. S. Ogden, *Inorg. Chem.*, **11**, 666 (1972).
(21) P. Kündig, M. Moskovits, and G. A. Ozin, *J. Mol. Struct.*, **14**, 137 (1972).
(22) (a) E. P. Kündig, D. McIntosh, M. Moskovits, and G. A. Ozin, *J. Am. Chem. Soc.*, **95**, 7234 (1973); (b) H. Huber, P. Kündig, M. Moskovits, and G. A. Ozin, *Nature (London), Phys. Sci.*, **235**, 98 (1972).
(23) H. A. Jahn and E. Teller, *Proc. R. Soc. London, Ser. A*, **161**, 220 (1937).
(24) H. Hallam, Ed., "Vibrational Spectra of Trapped Species", Wiley, London, 1973.
(25) D. McIntosh and M. R. Peterson, Vibrational Analysis Programmes, QCPE, 1977.
(26) F. A. Cotton and C. S. Kraihanzel, *J. Am. Chem. Soc.*, **84**, 4432 (1962).
(27) A. J. L. Hanlan, A. B. P. Lever, H. B. Gray, and G. A. Ozin, *Inorg. Chem.*, in press.
(28) (a) I. H. Hillier, M. F. Guest, B. R. Higginson, and D. R. Lloyd, *Mol. Phys.*, **27**, 215 (1975); (b) I. H. Hillier and U. R. Saunders, *ibid.*, **22**, 1025 (1971); (c) J. C. Demuynck, *Chem. Phys. Lett.*, **45**, 74 (1977); (d) J. C. Demuynck and A. Veillard, *Theor. Chim. Acta*, **28**, 241 (1973); (e) D. R. Lloyd and E. W. Schlag, *Inorg. Chem.*, **8**, 2544 (1969).
(29) (a) A. F. Schreiner and T. L. Brown, *J. Am. Chem. Soc.*, **90**, 3366 (1968); (b) H. B. Jansen and P. Ros, *Theor. Chim. Acta*, **34**, 85 (1974); (c) E. J. Baerends and P. Ros, *Mol. Phys.*, **30**, 1735 (1975); (d) R. Osman, C. S. Ewig, and J. R. Van Wazer, *Chem. Phys. Lett.*, **39**, 27 (1976); (e) T. Zeigler, *Acta Chem. Scand., Ser. A*, **28**, 29 (1974); (f) see also ref 28a–c.
(30) N. A. Beach and H. B. Gray, *J. Am. Chem. Soc.*, **90**, 5713 (1968).
(31) A. E. Martell, Ed., "Coordination Chemistry", Vol. 1, Van Nostrand-Reinhold, New York, 1971.
(32) H. Huber, E. P. Kündig, M. Moskovits, and G. A. Ozin, *J. Am. Chem. Soc.*, **95**, 332 (1973).
(33) H. Huber, E. P. Kündig, M. Moskovits, and G. A. Ozin, *Can. J. Chem.*, **50**, 2385 (1972).
(34) E. P. Kündig, M. Moskovits, and G. A. Ozin, *Can. J. Chem.*, **51**, 2710 (1973).
(35) E. P. Kündig, M. Moskovits, and G. A. Ozin, *Can. J. Chem.*, **50**, 3587 (1972).
(36) D. McIntosh and G. A. Ozin, *J. Am. Chem. Soc.*, **98**, 3167 (1976).
(37) L. Malatesta, G. Caglio, and M. Angoletta, *Chem. Commun.*, 532 (1970).
(38) N. N. Kautaradze and N. P. Sokolova, *Dokl. Akad. Nauk SSSR*, **168**, 140 (1966).
(39) C. R. Guerra and J. H. Schulman, *Surf. Sci.*, **7**, 229 (1967).
(40) (a) P. K. Hansma, W. C. Kaska, and R. M. Laine, *J. Am. Chem. Soc.*, **98**, 6064 (1976); (b) R. M. Laine, 172nd National Meeting of the American Chemical Society, San Francisco, Calif., Sept 1976 (private communication).
(41) C. W. Garland, R. C. Lord, and P. F. Troiano, *J. Phys. Chem.*, **69**, 1188 (1965).
(42) J. F. Harrod, R. W. Roberts, and E. F. Rissman, *J. Phys. Chem.*, **71**, 343 (1967).
(43) F. S. Baker, A. M. Bradshaw, J. Pritchard, and K. W. Sykes, *Surf. Sci.*, **12**, 426 (1968).
(44) H. C. Eckstrom, G. C. Possley, and S. E. Hannum, *J. Chem. Phys.*, **52**, 5435 (1970).
(45) C. E. O'Neill and D. J. C. Yates, *J. Phys. Chem.*, **65**, 901 (1961).
(46) L. Lynds, *Spectrochim. Acta*, **20**, 1369 (1964).
(47) M. Moskovits and G. A. Ozin, *Appl. Spectrosc.* **26**, 481 (1972).

Contribution from Lash Miller Chemical Laboratories and Erindale College, University of Toronto, Toronto, Ontario, Canada

Bimetal Atom Chemistry. 2. Selective Bimetallic Photoaggregation of Ag and Cr Atoms to Very Small Clusters, Cr_nAg_m

GEOFFREY A. OZIN* and WERNER E. KLOTZBÜCHER

Received August 9, 1978

Silver and chromium form a binary alloy system of the low-miscibility class. By employment of Ag/Cr atom 10–12 K matrix codepositions, selective atomic excitation, and optical spectroscopy it is demonstrated that very small, naked bimetallic clusters of the form AgCr and Ag_2Cr can be selectively photogenerated and identified in the presence of the parents $Ag_{2,3}$ and $Cr_{2,3}$. Extended Hückel molecular orbital techniques are employed to probe the electronic and bonding properties of these unique bimetallic combinations. The implications of these observations for two electronically disparate metals to the left and right of the transition series to Sinfelt's concepts of alloy and bimetallic cluster catalysis are briefly discussed.

Introduction

Highly dispersed, supported bimetallic and trimetallic clusters are proving to be extremely effective catalysts in the gas–oil–petroleum industries, particularly for such processes as hydrocracking and naphtha re-forming.[1]

Up to the present time, supported multimetallic samples have usually been prepared by coimpregnation and subsequent reduction of an appropriate combination of metal salts.[2b] Unsupported samples may be prepared by similar metal salt reduction techniques,[2c] evaporation of the pure metals,[2d] and leaching of a bulk alloy to give a selected bimetallic catalyst with a high surface area.[2e] However, a question of central concern in high-dispersion multimetallic catalyst systems, especially for mixtures of salts which display little if any miscibility in the bulk phase, is whether one obtains the metal components as separate particles or rather as "multimetallic

0020-1669/79/1318-2101$01.00/0